Electron velocity overshoot and nonequilibrium phonons in a GaAs-based *p-i-n* nanostructure studied by transient subpicosecond Raman spectroscopy

E. D. Grann and K. T. Tsen
Department of Physics and Astronomy, Arizona State University, Tempe, Arizona 85287

D. K. Ferry
Department of Electrical Engineering, Arizona State University, Tempe, Arizona 85287

A. Salvador, A. Botcharev, and H. Morkoc
Coordinated Science Laboratory, University of Illinois, Urbana, Illinois 61801
(Received 3 August 1995; revised manuscript received 8 December 1995)

Transient subpicosecond Raman spectroscopy has been used to study electron velocity overshoot as well as nonequilibrium phonons in a GaAs-based *p-i-n* nanostructure under the application of high electric fields. Both electron distribution functions and nonequilibrium phonon populations were directly obtained in the velocity overshoot regime for a variety of electric field intensities and for different electron densities. All of our experimental results are compared with ensemble Monte Carlo calculations and good agreement is achieved.

I. INTRODUCTION

The behavior of electrons in semiconductors has long been studied for both fundamental and technological reasons. In particular, the transport properties of electrons under the influence of an electric field have been extensively investigated experimentally as well as theoretically.[1] As the size of semiconductor devices gets smaller, the time scale important for device operation becomes shorter. The recent development of laser sources with picosecond and subpicosecond pulse widths has led to optical methods which can directly probe electron transport phenomena on very short time scales. In these short time regimes, the transport properties of electrons are known to be quite different from those observed under steady state conditions.[2] Understanding these nonequilibrium phenomena is the key to taking advantage of these novel transient transport properties.

An important parameter in a semiconductor is the electron distribution function. On very short time scales, electrons which are photoexcited in a polar semiconductor such as GaAs exhibit extremely nonequilibrium distributions, far from either a Maxwell-Boltzmann or Fermi-Dirac distribution. The application of a high external electric field enhances the nonequilibrium nature of the electron distribution. The majority of work on nonequilibrium distribution functions in semiconductor devices has been theoretical. Solution of the Boltzmann equation or Monte Carlo simulations provide insight into the nature of the distribution function for electrons moving in an electric field. The Boltzmann equation is, in general, very difficult to solve and is less applicable in the circumstances of short time scales and high electric fields. For this reason, most theoretical descriptions of nonequilibrium distribution functions involve Monte Carlo simulations.[3]

Experimentally, it is difficult to directly measure the distribution function of electrons in a semiconductor. A common technique used to investigate nonequilibrium electron distributions in semiconductors is time-resolved luminescence spectroscopy.[4] The recombination luminescence of excited electron-hole pairs provides information about the product of the electron and hole distribution functions. Another technique, time-resolved differential transmission spectroscopy,[5] probes the sum of the electron and hole distribution functions. These two techniques have been used for probing carrier distribution functions in both bulk GaAs and GaAs quantum well structures. We note that it is very difficult for these methods to decouple the distribution of the electrons from that of the holes, particularly on very short time scales.

On the other hand, Raman scattering from single-particle excitations has long been known as an effective probe of the velocity distribution of electrons moving under the influence of an electric field in semiconductors. Mooradian and McWhorter[6] first demonstrated this technique using a Q-switched Nd:YAG laser to probe the velocity distribution of electrons in n-GaAs ($n \cong 10^{15}$ cm^{-3}) at liquid helium temperatures and for applied fields up to 2 kV/cm. They tried to describe the electron distribution by a drifted Maxwellian distribution. Ralph and Wolga[7] used single-particle scattering (SPS) difference spectra to monitor changes in the electron distribution function in a GaAs-based n^+-n^--n^+ device for fields up to 1 kV/cm. A Kr-ion-pumped dye laser operating near but below the band gap was used to scatter from the electrically injected electrons under both forward and reverse biased conditions. They found that a drifted Maxwellian fit their difference spectra provided that the effect of resonance enhancement was included. Grann *et al.*[8] used transient picosecond Raman spectroscopy to determine electron drift velocities as well as electron distribution functions in undoped, bulk GaAs for a variety of applied electric field intensities, photon energies, and photoexcited electron densities at $T \cong 80$ K. They found that for an excitation photon energy of $\hbar\omega = 1.951$ eV, increasing the carrier concentration from $\cong 10^{17}$ to 10^{18} cm^{-3} caused the electron distribution to change from an extremely nonequilibrium one to a drifted Fermi-Dirac distribution characterized by a drift velocity and

0163-1829/96/53(15)/9838(9)/$10.00 © 1996 The American Physical Society

a temperature much higher than that of the lattice. Recently, Grann *et al.*[9] used transient subpicosecond Raman spectroscopy to interrogate electron transport in the regime of electron velocity overshoot.

In GaAs, highly energetic electrons thermalize with the lattice via the emission of LO phonons. Kim and Yu[10] used transient subpicosecond Raman spectroscopy to study the relaxation mechanisms of hot electrons and phonons in GaAs without an applied electric field. They found that within the first picosecond after photoexcitation, intervalley scattering was the dominant cooling process for the electrons. This caused the effective temperature of the nonequilibrium phonons to temporarily overshoot that of the hot electrons.

In this paper we report on the direct determination of the electron distribution functions and nonequilibrium LO phonon populations in undoped GaAs in the presence of high electric fields using transient subpicosecond Raman spectroscopy. Our experiments probed the electron dynamics within the first picosecond after electrons were photoexcited into the conduction band in GaAs and then accelerated by the high applied electric field. On this time scale ($\cong$600 fs), electron transport is in the so-called velocity overshoot regime.[5,11,12] Electron velocity overshoot is a short-time scale, high-electric field phenomenon in which electrons travel through a semiconductor with average velocities higher than their steady-state values. The electron distribution functions, drift velocities, and nonequilibrium LO phonon populations have been studied as a function of electric field intensity and electron density. All of our experimental results are compared with ensemble Monte Carlo (EMC) simulations.

II. SAMPLE AND EXPERIMENTAL TECHNIQUE

The sample was grown by molecular beam epitaxy on a (001)-oriented GaAs substrate. The detailed description of the sample has been presented elsewhere.[8] The p-type and n-type layers formed the positive and negative sides of what is effectively a parallel plate capacitor. The high electric fields were established across the intrinsic region of a GaAs-based p-i-n nanostructure. The electric field in the intrinsic region is given by $E=(V_{\mathrm{bi}}-V_{\mathrm{app}})/d$, where V_{bi} is the device's built-in voltage, V_{app} is the applied voltage, and d is the thickness of the intrinsic region. The photocurrent was monitored and was not allowed to exceed 0.5 mA in order to inhibit possible domain formation.[13] The laser pulses used in this experiment had an energy of 1.951 eV and a pulse width of $\cong$600 fs. They were generated by a double-jet DCM dye laser which was synchronously pumped by the second harmonic of a mode-locked Nd:YAG laser operating at 76 MHz. The energy of the incident photons was chosen to be $\hbar\omega_L=1.951$ eV, very close to the $E_0+\Delta$ band gap of GaAs, to take advantage of the resonance enhancement. We note that at this incident photon energy, electrons were generated from the heavy-hole, light-hole, and split-off hole valence bands. In addition, at this incident photon energy, the contributions of the E_0 and $E_0+\Delta$ band gap luminescences in GaAs to the spectrum are easily identified and subtracted out. The photoexcited carrier density was adjusted by varying the spot size of the laser on the sample. Because the band gap of the AlAs layer in the p-type region is greater than 1.951 eV, both the incident and scattered light were unaffected by the presence of the p-type layer. All the experiments were carried out at $T=80$ K.

The SPS experiments were conducted in the $Z(X,Y)\bar{Z}$ scattering geometry, where $Z=(001)$, $X=(100)$, and $Y=(010)$. This orientation scatters light from only single-particle excitations associated with spin density fluctuations.[14,15] The SPS cross section is inversely proportional to the effective mass (see later discussion); therefore our experiment predominantly probes electron transport in the Γ valley even though holes are simultaneously present. In our SPS experiments, photons from the same pulse were used to both excite and probe electrons, hence, the results represent an average over the laser pulse width. We note that under reverse-bias conditions, our backscattering geometry probes the electron distribution functions along the direction of $-\mathbf{E}$. In order to easily observe the behavior of the LO phonons, a $Z(X',X')\bar{Z}$ scattering geometry was used, where $Z=(001)$, $X'=(110)$.

The scattered light was collected and analyzed by a double monochromator and a CCD detector. For the SPS experiments, the internal slits of the monochromator were closed down to 2 mm in order to reduce the stray light. This enabled us to scan to ±100 cm^{-1} of the laser line. For the hot phonon experiments, the internal slits were wide open ($\cong$8 mm), allowing a spectral coverage of $\approx$100 cm^{-1}.

III. EXPERIMENTAL RESULTS AND ANALYSIS

Figure 1(a) shows a typical SPS spectrum of the mesa-like GaAs p-i-n sample taken at $T\approx80$ K and $n\approx10^{18}$ cm^{-3} for an electric field intensity of $E=15$ kV/cm. The spectrum lies on top of a background due to electron–hole recombination luminescence at the E_0 band gap.[8,9] The background luminescence can be very well fit by an exponential function, as shown by the solid line in Fig. 1(a). To obtain the SPS contribution, this E_0 band-gap luminescence background was first subtracted from the Raman spectrum. Then, the $E_0+\Delta$ band-gap luminescence was subtracted in the following way: The $E_0+\Delta$ band-gap luminescence was found to peak at $\approx$600 cm^{-1} from the laser line on the Stokes side.[8] Our subtraction procedure assumed that contributions to the measured Raman spectrum for energy shifts greater than $\approx$600 cm^{-1} were due solely to the $E_0+\Delta$ band-gap luminescence.[16] The luminescence was also considered to be symmetric about its peak; its shape was estimated by reflecting the spectrum greater than 600 cm^{-1} about its peak as shown in Fig. 1(b). The $E_0+\Delta$ band-gap luminescence was thus subtracted from the Raman spectrum. All of the SPS spectra shown later have had the E_0 and $E_0+\Delta$ band-gap luminescences subtracted in this way. Figure 2 shows the SPS spectra of the p-i-n GaAs sample for various electric field intensities and electron density of $n\approx10^{18}$ cm^{-3}.

We now convert the SPS spectra in Fig. 2 into electron distribution functions along the direction of the wave-vector transfer $\mathbf{q}\equiv\mathbf{k}_i-\mathbf{k}_s$, where $\mathbf{k}_i,\mathbf{k}_s$ are the wave vectors of the incident and scattered photons, respectively. For light scattering from electrons in semiconductors, in the effective mass approximation, momentum and energy conservation require that the following relation hold:

$$\hbar\omega=\hbar\mathbf{q}\cdot\mathbf{V}+\frac{\hbar^2q^2}{2m^*}, \quad (1)$$

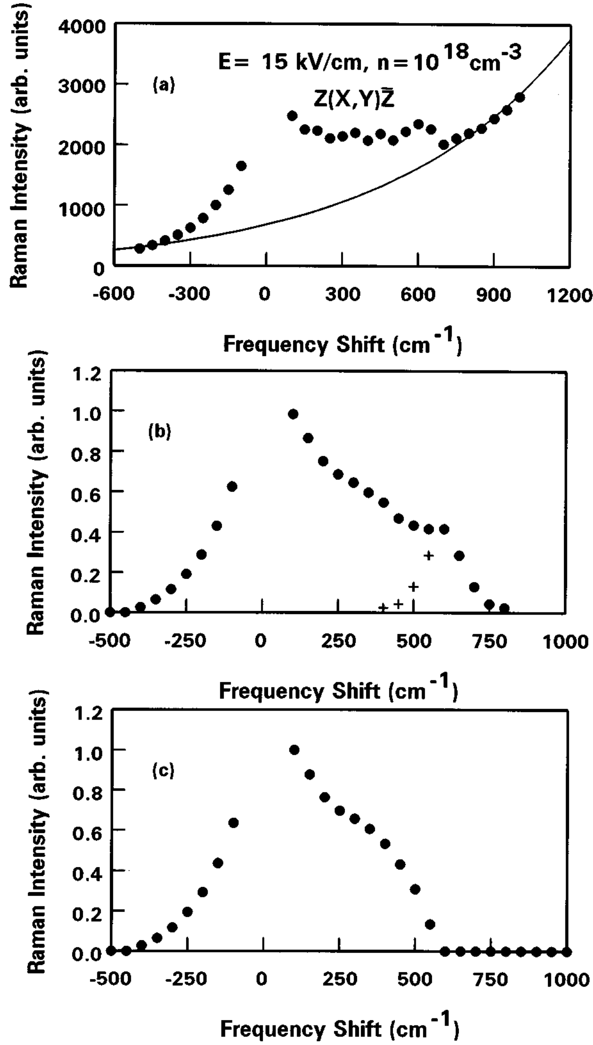

FIG. 1. (a) A typical SPS spectrum for a GaAs-based p-i-n nanostructure semiconductor taken at $T=80$ K, $E=15$ kV/cm, and for $n \cong 10^{18}$ cm^{-3}. The solid curve represents luminescence from the E_0 gap of GaAs. (b) SPS spectrum after the subtraction of luminescence from the E_0 gap. The crosses show the estimated luminescence from the $E_0+\Delta$ gap of GaAs. (c) SPS spectrum after the subtraction of luminescence from both the E_0 and $E_0+\Delta$ gaps of GaAs.

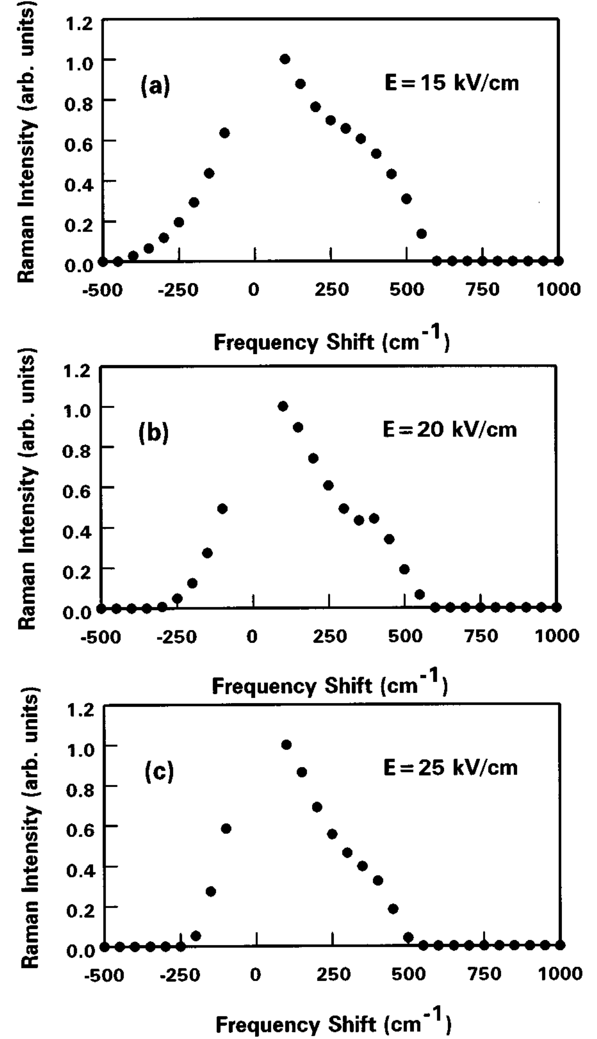

FIG. 2. SPS spectra (after the subtraction of E_0 and $E_0+\Delta$ gap luminescences) for a GaAs-based p-i-n nanostructure semiconductor taken at $T=80$ K, $n \cong 10^{18}$ cm^{-3} and for electric field intensities (a) $E=15$ kV/cm; (b) $E=20$ kV/cm; (c) $E=25$ kV/cm, respectively.

where $\hbar w$ is the energy shift of the scattered photons, m^* is the effective mass of the electron, and $\mathbf{V}$ is the velocity of the electrons. Next, we consider the following simple expression for the SPS cross section for scattering from spin density fluctuations where the laser pulse width is $\geqslant 500$ fs, the effects of collisions are neglected, and the electron distribution function is assumed to be nondegenerate:[17]

$$\frac{d^2\sigma}{d\omega\, d\Omega} = \left(\frac{e^2}{m^* c^2}\right)^2 \int d^3k\; n(\mathbf{k}) |M_{\mathrm{SDF}}(\mathbf{k})|^2 \times \delta\left(\omega - \frac{\varepsilon_{\mathbf{k}+\mathbf{q}} - \varepsilon_{\mathbf{k}}}{\hbar}\right), \qquad (2)$$

where e is the charge on the electron, c is the speed of light, $n(\mathbf{k})$ is the electron distribution function, $|M_{\mathrm{SDF}}(\mathbf{k})|$ is the electron momentum matrix element, and d is an energy conserving delta function. If one neglects the $\mathbf{k}$ dependence of the matrix element, then

$$\frac{d^2\sigma}{d\omega\, d\Omega} \propto \left(\frac{1}{m^*}\right)^2 \int d^3k\; n(\mathbf{k})\, \delta\left(\omega - \frac{\varepsilon_{\mathbf{k}+\mathbf{q}} - \varepsilon_{\mathbf{k}}}{\hbar}\right). \qquad (3)$$

Equation (3) states that the Raman scattering cross section at a given w [and therefore a given $V_q \equiv (\mathbf{V}\cdot\mathbf{q})/|\mathbf{q}|$] is directly proportional to the number of electrons that have a velocity component V_q in the direction of the wave-vector transfer $\mathbf{q}$ given by Eq. (1), irrespective of their velocity components perpendicular to $\mathbf{q}$. In other words, the SPS cross section is directly proportional to the electron distribution function along the direction of wave-vector transfer.

We note that the effective mass of an electron is not constant throughout the Γ valley. In semiconductors like GaAs, the higher the electron velocity in the Γ valley, the heavier the electron's effective mass. By integrating Eq. (3) over the two directions perpendicular to $\mathbf{q}$ using a two-dimensional density of states, we find that the scattering cross section is

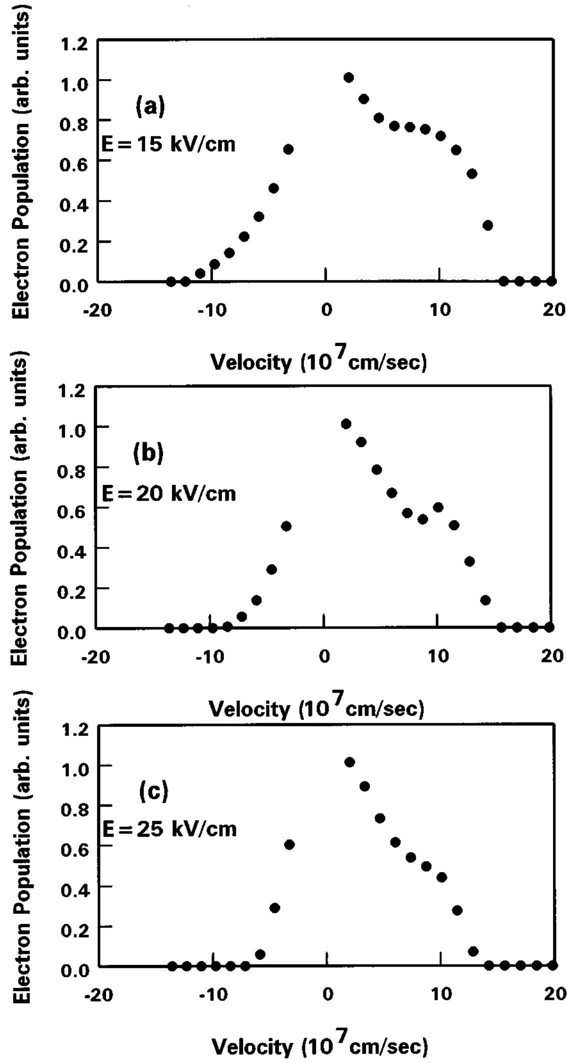

FIG. 3. The electron distribution functions obtained from SPS spectra of Fig. 3 for electron density $n \cong 10^{18}$ cm^{-3} and for electric field intensities (a) $E=15$ kV/cm, (b) $E=20$ kV/cm, (c) $E=25$ kV/cm, respectively.

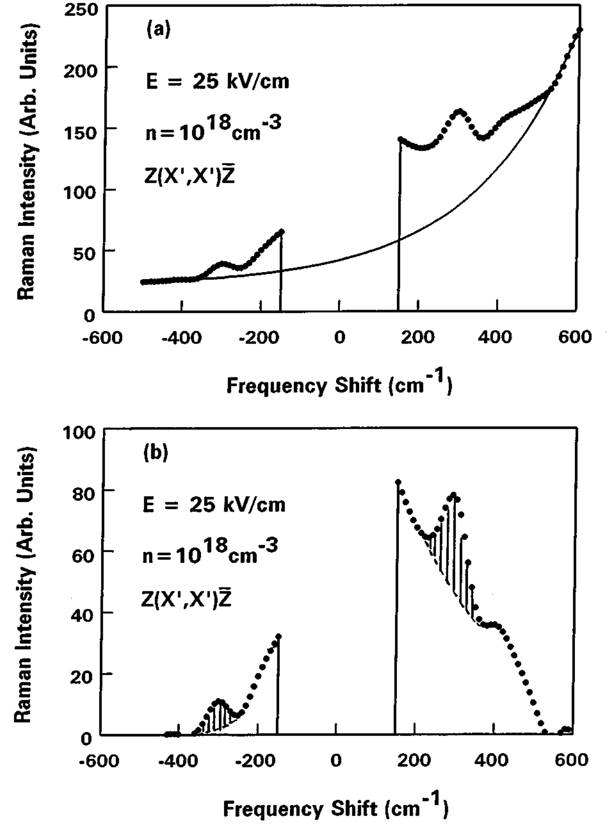

FIG. 4. (a) A typical Raman spectrum showing the observation of nonequilibrium LO phonons around ± 300 cm^{-1}. The solid curve corresponds to the luminescence from the E_0 gap of GaAs. (b) Raman spectrum of (a) after the subtraction of luminescence background. The shaded areas around ± 300 cm^{-1} were used to calculate the nonequilibrium phonon populations.

inversely proportional to the electron's effective mass m^*. Therefore, the SPS cross section is proportional to the electron distribution function along the wave-vector transfer **q** and is also inversely proportional to the effective mass of the electron.

Because of the very high drift velocities in our experiment, the effects of band nonparabolicity must be considered in both Eqs. (3) and (1). Currently, the accepted model for treating nonparabolicity is the Kane **k**·**p** model.[18,19] The validity of the Kane model can be illustrated by the "maximum" attained velocity (as a result of the band's becoming quite linear in k) of 1.2×10^8 cm/s, which is quite close to the value obtained from full-zone empirical pseudopotential calculations.[20–22] Therefore, nonparabolicity of the conduction band in GaAs was accounted for approximately[23] by replacing m^* with $m^* = m_c^*(1+2E/E_g)$,[18] where m_c^* is the electron effective mass at the Γ point, E is the energy of the electron, and E_g is the band gap of GaAs. The energy of the electron is given by $E=\frac{1}{2}m^* V^2$. We write $E=\frac{1}{2}m^*(V_q^2+V_x^2+V_y^2)$, where V_x and V_y are the electron velocity components perpendicular to the direction of **q**. Since electrons are accelerated in the direction of wave-vector transfer **q** only, it is expected that the x and y components of electron velocity distribution can be very well approximated by the electron distribution function taken in bulk GaAs under the same experimental conditions as ours except that the applied electric field is zero. It has been shown by Kim and Yu[10] that the electron effective temperatures in bulk GaAs under almost the same experimental conditions as ours and $\mathbf{E}=0$ were $T_e \approx 600$ K. To a good approximation, this means that the contribution to the electron energy from either the x or y velocity components is $\cong \frac{1}{2}k_B T_e$, where k_B is the Boltzmann constant. Therefore, we have

$$E \cong k_B T_e + \tfrac{1}{2} m^* V_q^2, \qquad (4)$$

where $T_e = 600$ K.

The effective mass of the electron as a function of electron velocity is then given by

$$m^* \cong \frac{E_g m_c^* (1+2k_B T_e/E_g)}{E_g - m_c^* v_q^2}. \qquad (5)$$

To convert the experimentally measured SPS cross section into the electron distribution function along the direction of

TABLE I. Measured electron drift velocities for various electric field intensities and electron density of $n=1\times10^{8}$ cm^{-3} are compared with EMC simulations.

Electron Density / V_d / E	n=1x10^{18} cm^{-3}			
	Drift Velocity (cm/sec) 600 fs	EMC (cm/sec) 600 fs	Drift Velocity (cm/sec) 3 ps	EMC (cm/sec) 3 ps
15 kV/cm	(3.6±0.7)x10^7	(2.9±0.3)x10^7	(1.0±0.2)x10^7	(2.2±0.6)x10^6
20 kV/cm	(3.8±0.8)x10^7	(2.9±0.3)x10^7	NA	NA
25 kV/cm	(2.9±0.6)x10^7	(3.1±0.3)x10^7	(1.6±0.3)x10^7	(9.7±2.3)x10^6

wave-vector transfer, we first use Eqs. (1) and (5) to convert the Raman shift w into a corresponding electron velocity V_q. The electron distribution functions along the **q** direction were then determined by multiplying the measured SPS cross section by the velocity-dependent effective mass m^* [Eq. (5)]. We note that the effective electron temperature T_e in the x and y directions may vary with the electric field intensity. However, this should not change the results of our analysis very much because we have found that the conversion of both the Raman signal to electron distribution and the frequency shift to electron velocity are not sensitive to the effective temperature of the electron T_e. The electron distributions thus obtained are shown in Fig. 3 for various electric field intensities and for electron density $n\cong10^{18}$ cm^{-3}. The drift velocity for each electron distribution function was calculated in a straightforward way by taking a weighted average over the electron velocity distribution. The deduced drift velocities are shown in Table I.

In general, the deduced drift velocities for an electron density of $n\cong10^{18}$ cm^{-3} are systematically smaller than those for $n\cong10^{17}$ cm^{-3}.[9] This is due to the fact that the momentum randomization is much larger for the higher electron density than for the lower electron density. For convenience, we have also shown in Table I the drift velocities obtained under exactly the same experimental conditions except that the laser pulse width was 3 ps. The reduction in the electron drift velocities found in the 3-ps data, *vis-à-vis* the 0.6-ps data is clear support for the existence of velocity overshoot. In such situations, the carriers respond to the high electric field, rising to a velocity characteristic of the momentum relaxation time of the cold carriers, then relax to a lower velocity as the distribution is heated. It is important to note that the distribution function is not isotropic in the high field (within the central Γ valley), and that is why it is important to use a geometry in which the Raman scattering probes the carrier distribution function along the field. The presence of the nonequilibrium phonons complicates the cooling processes, and it is well known that this leads to a "phonon bottleneck" which hinders the cooling of the electron distribution within the Γ valley. The presence of the high electric field modifies this role. Normally, the electron velocity overshoot would be over with within the first picosecond, and it is only the fact that the Raman scattering samples carriers in the Γ valley where the phonon bottleneck is present that allows a nonequilibrium velocity to still be detected at 3 ps.

Figure 4 shows a typical Raman spectrum for a GaAs p-i-n nanostructure taken at $T\approx80$ K, $n\cong10^{18}$ cm^{-3}, $E=15$ kV/cm, and in the $Z(X',X')\bar{Z}$ scattering geometry. The spectrum contains three parts. One is the luminescence background due to electron–hole recombination at the E_0 band gap of GaAs. Again it is very well fit by an exponential function. Another is the structure around the laser line which is the SPS contribution. The third part is the small structures centered about ±300 cm^{-1} which are due to scattering of light by the plasmon–LO phonon coupled modes. As argued by Kim and Yu,[9] for electron concentrations of $\cong10^{17}$ cm^{-3} and greater, the plasmon frequency becomes very close to the LO phonon frequency; the plasmons and the LO phonons are therefore indistinguishable and, for brevity, we refer to these plasmon-LO phonon coupled modes as LO phonons. The population of nonequilibrium LO phonons can be obtained in the following way:

$$n(\omega_{\rm LO})=\frac{1}{I_S/I_{AS}-1}, \tag{6}$$

where $\omega_{\rm LO}$ is the LO phonon frequency, and I_S, I_{AS} are the intensities of the Stokes and anti-Stokes LO phonon Raman lines, respectively. The measured population of nonequilibrium LO phonons for various electric field intensities and carrier concentrations are shown in Table II. We have found that, in general, the measured LO phonon population increases when either the photoexcited electron density or the electric field intensity increases, as expected.

We note that since the penetration depth of the laser is about 0.3 μm, a significant number of electrons can leave this laser-probed region or scattering volume and be collected at the contact even if their average velocities in the direction of wave-vector transfer **q** are of the order of 10^7 cm/s. In addition, once the electrons suffer intervalley scattering to the L valleys, they become electrons of very low kinetic energies; because of the small excess energy and the large effective mass of electrons in the L valley, the range of LO phonon wave vectors these electrons emit during their thermalization toward the bottom of L valley is beyond the wave vector of LO phonons "probed" in our Raman scattering experiments, i.e., $q=7.1\times10^5$ cm^{-1}. Furthermore, these electrons will not return to the Γ valley until about 2 ps.[10,24–27] Because the laser pulse width used in our experiment was $\cong$600 fs, such an intervalley scattering of electrons will reduce the nonequilibrium phonon populations probed in our experiment. Based upon the above arguments, we can now explain our experimental results on the nonequilibrium phonon populations.

The applied electric field has two effects on the observed phonon population. The first is to accelerate the electrons to higher energies where they emit more LO phonons. The second effect is that because of acceleration by the electric field these highly energetic electrons will leave the scattering volume or suffer intervalley scattering and thus fewer LO phonons can be detected. The interplay between these two competing effects can be seen from the observed field-dependent nonequilibrium LO phonon populations in Table II. For $n\cong10^{16}$ cm^{-3}, there is very little momentum randomization, so the electron drift velocity increases dramatically with an increase in the electric field intensity. The increase in the LO phonon population due to electron acceleration is

TABLE II. Measured nonequilibrium LO phonon populations for various electric field intensities and electron densities are compared with EMC simulations.

Electron Density	$n=10^{16}$ cm^{-3}		$n=10^{17}$ cm^{-3}		$n=10^{18}$ cm^{-3}	
Phonon. Pop. / E	$n(\omega_{LO})$	EMC	$n(\omega_{LO})$	EMC	$n(\omega_{LO})$	EMC
15 kV/cm	0.181±0.02	1.32 x10^{-2}	0.298±0.03	7.94x10^{-2}	0.413±0.04	0.381
20 kV/cm	0.146±0.01	1.57x10^{-2}	0.326±0.03	7.94x10^{-2}	0.499±0.05	0.610
25 kV/cm	0.119±0.01	8.81x10^{-3}	0.445±0.04	0.114	0.615±0.06	0.543

relatively small compared to the decrease in the LO phonon population as a result of electrons leaving the scattering volume, or suffering intervalley scattering. This causes the observed population of the LO phonons to decrease with an increase in the electric field intensity. On the other hand, for the higher electron densities such as $n \cong 10^{17}$ and 10^{18} cm^{-3}, the relatively larger effects of momentum randomization causes the electron drift velocity to increase only moderately with the field. The increase in LO phonon populations due to electron acceleration becomes large compared with the decrease of LO phonon population due to electrons leaving the scattering volume or suffering intervalley scattering. Therefore at such high electron densities the LO phonon population increases as the electric field increases.

IV. MONTE CARLO SIMULATIONS

Simulations of the laser-excited plasma were carried out by the EMC technique.[28] In this simulation, only the electrons were considered, as the population of the polar modes was of primary interest. Nonparabolic energy bands were assumed for the various conduction bands, and all normal scattering processes were included. Interaction among the electrons was treated by a molecular-dynamics simulation technique, including the role of the exchange energy.[29,30] Particles are assumed to be generated in the intrinsic region of the GaAs p-i-n structure, with a positional probability determined by the attenuation of absorption into the material from the front surface. These particles are then allowed to evolve, and cool, under the influence of the built-in electric field. Special treatment is accorded to the particles as they reach the heterojunction interfaces at the ends of the central portion of the structure. Particles with sufficient energy to surmount the heterostructure band discontinuity are allowed to move into the AlAs, and are removed from the simulation ensemble. Those with insufficient energy to surmount the barrier are assumed to undergo diffusive interface scattering, thus being reflected back into the central region. The Raman signal is then estimated by computing the population of both electrons and phonons, and weighting them by the absorption undergone in photon transmission through the active area.

On the short time scales, which depend upon the system being modeled, the electron distribution undergoes a significant perturbation in the typical time between scattering events. During the first picosecond of relaxation, a finite density of electrons (holes) will lose about 10% of their energy in each 0.1 ps through the emission of a phonon. The phonon scattering is treated in the semiclassical Fermi golden rule model, with the final states of the scattering process being selected by a weighted random selection, as in normal Monte

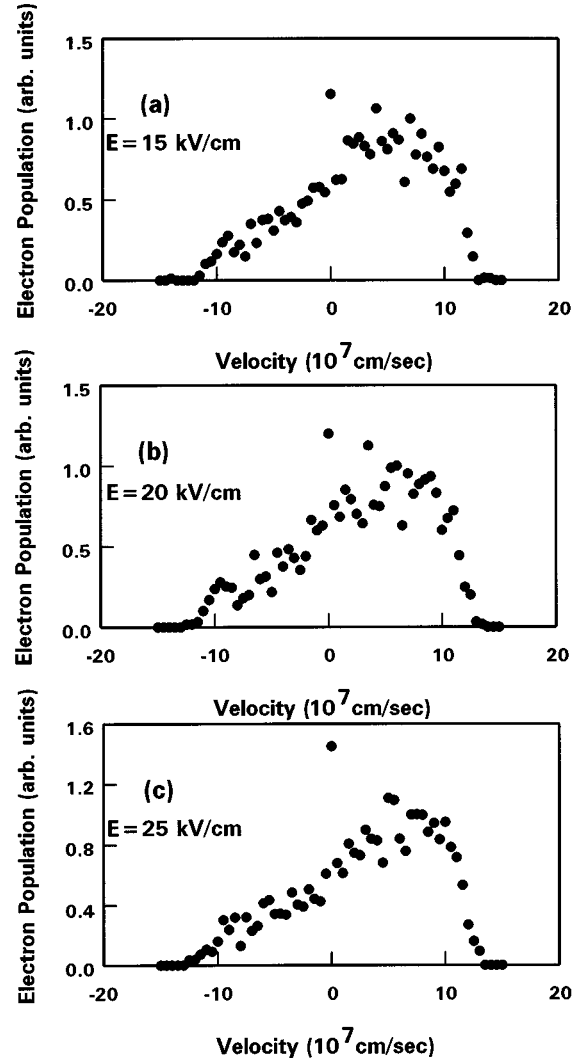

FIG. 5. Electron distribution functions from EMC simulations for a GaAs-based p-i-n nanostructure semiconductor, for $n \cong 10^{18}$ cm^{-3} and electric field intensities (a) $E=15$ kV/cm, (b) $E=20$ kV/cm, (c) $E=25$ kV/cm, respectively.

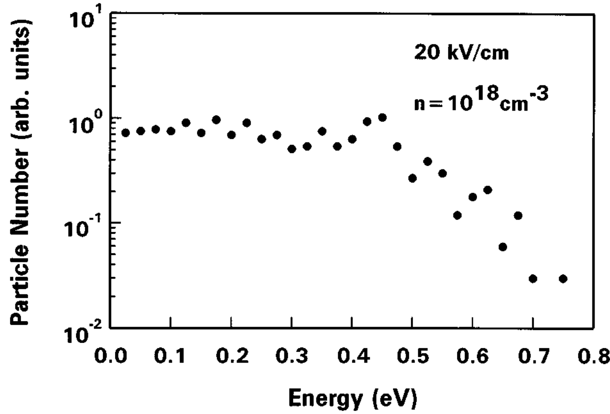

FIG. 6. The total number of electrons as a function of electron energy obtained from EMC simulations for a GaAs-based p-i-n nanostructure semiconductor, for $n \cong 10^{18}$ cm^{-3} and at a time of 0.7 ps, that is just past the peak of the laser pulse.

Carlo techniques. During this initial decay, the plasma is modeled by an ensemble of electrons, and this approach has been successfully vectorized. Carrier-carrier scattering, however, is a multi-carrier interaction which requires that these other carriers be available for the interaction. In general, a treatment similar to that for the phonons is possible only if the Coulomb interaction is treated as "instantaneous." For this reason, we treat the Coulomb interaction via a real-space molecular dynamics approach.[31]

Modeling of the nonequilibrium phonons is handled within the EMC procedure by a secondary self-scattering and rejection process pioneered by Lugli *et al.*[32] The buildup of the phonon population through emission and absorption processes is monitored throughout the simulation. The difference between the instantaneous value, for a given momentum wave vector, and some prescribed maximum value is used for the rejection technique. The presence of the nonequilibrium phonons slows the energy decay of the hot carriers.

In Fig. 5, the carrier populations are plotted as a function of the electron velocity in the direction of wave-vector transfer in the p-i-n structure for the three values of electric field studied here. The three distributions look basically quite

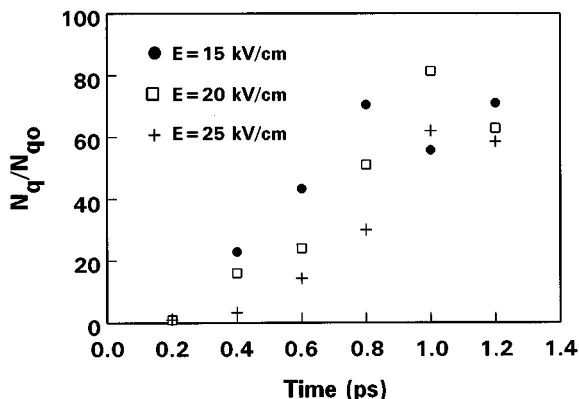

FIG. 7. Phonon populations (normalized to the equilibrium phonon population at $T=80$ K) as a function of time for $n \cong 10^{18}$ cm^{-3} and for three electric field intensities as indicated.

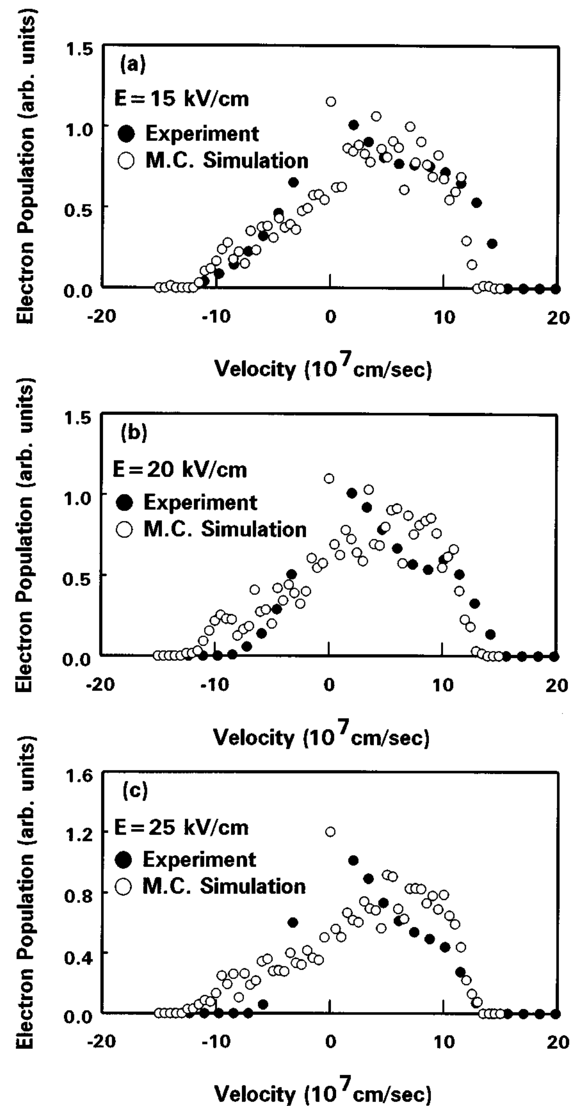

FIG. 8. Comparison of the measured electron distribution functions (closed circles) with EMC simulations (open circles) for $n \cong 10^{18}$ cm^{-3} and electric field intensities (a) $E=15$ kV/cm, (b) $E=20$ kV/cm, (c) $E=25$ kV/cm, respectively.

similar. However, the 15-kV/cm data has a higher overall population than the two higher fields (the same normalization is used for all three field values). At the higher fields, a greater fraction of the carriers is swept into the AlAs layers. Moreover, the skew of the distribution to large positive values of velocity is evident. The sharp cutoff occurring near 1.2×10^8 cm/s is a result of the strong nonparabolicity in the central Γ valley of the conduction band of GaAs. This is close to the maximum that can be achieved in these bands. For comparison, the distribution of the carriers as a function of their energy is plotted in Fig. 6 for a field of 20 kV/cm, and at a time point just past the peak of the laser pulse (0.7 ps). Because of the strong nonlinearity in the transport in the high fields, the average velocity of the distribution is a strong function of the time during the pulse. Finally, the phonon population is plotted in Fig. 7 as a function of time for the three values of the electric field. It is clear that the phonons are driven further from equilibrium in the higher fields. Moreover, the peak in the phonon population actually occurs

somewhat after the peak of the laser pulse, as might be expected, but this means that the Raman signal will average over this temporal distribution.

V. DISCUSSION

In Fig. 8, the measured electron distribution functions along the wave-vector transfer **q** or (−**E**) direction are compared with the EMC simulations. Qualitatively, the fit is good except in the regions of -1×10^8 and 1.2×10^8 cm/s. The deviation close to 1.2×10^8 cm/s is most probably due to the specific details of the hyperbolic band assumed in the EMC simulations. The large number of electrons in the negative velocity region (between -0.5×10^8 and -1.0×10^8 cm/s), which are not seen in the Raman experiment, is very likely due to the manner in which electron scattering at the interface is handled in the EMC simulations. In our EMC calculations, we assume that all the electrons that reach the AlAs–GaAs interface on the p-type region of the sample suffer diffusive scattering. If some of these electrons were allowed to suffer backscattering, the fit of the distribution function in the spectral range (from −0.5 to -1.0×10^8 cm/s) would improve; in addition, the discrepancy in the drift velocities between the experimental results and the EMC calculations presented in Table I would be reduced.

In Table II, the measured populations of nonequilibrium LO phonons are compared with the EMC simulations. We have found that the agreement is quite good for electron density of $n\cong10^{18}$ cm^{-3}. However, the EMC results are about a factor of 10 and 4 smaller than the measured values for electron densities $n\cong10^{16}$ and 10^{17} cm^{-3}, respectively. All of these results can be understood as follows: In the EMC calculations, the population of nonequilibrium LO phonons is an average over all the directions in **k** space. On the other hand, because of the applied electric field, the electron (and therefore the phonon) distribution function are expected to be very anisotropic in **k** space. The fact that the EMC calculations do not explain the measured nonequilibrium LO phonon populations is just a manifestation of such an anisotropic effect. This anisotropic effect is the largest for an electron density of $n\approx10^{16}$ cm^{-3} because this concentration has the smallest momentum randomization and as a result the largest anisotropic electron and phonon distribution functions. As the electron density increases to 10^{18} cm^{-3}, the anisotropic effect becomes less important as a result of stronger momentum randomization. This explains why the fit between the EMC calculations and the measured populations of nonequilibrium LO phonons gets better as the electron density increases from $n\approx10^{16}$ to $n\approx10^{18}$ cm^{-3}.

VI. CONCLUSIONS

We have used transient subpicosecond Raman spectroscopy to interrogate electron transport properties in a GaAs-based nanostructure semiconductor under the application of an electric field. Electron distribution functions, electron drift velocities and nonequilibrium LO phonons in the velocity overshoot regime have been directly measured as a function of electric field intensity and electron density. Our experimental results are in agreement with the EMC calculations.

ACKNOWLEDGMENT

This work was supported in part by the National Science Foundation under Grant No. DMR-9301100.

[1] E. M. Conwell, *High Field Transport in Semiconductors* (Academic, New York, 1967).

[2] T. J. Maloney and J. Frey, J. Appl. Phys. **48**, 781 (1977).

[3] See, for example, M. A. Osman and D. K. Ferry, Phys. Rev. B **36**, 6018 (1987).

[4] J. Shah, in *Hot Carriers in Semiconductor Nanostructures*, edited by J. Shah (Academic, Boston, 1992), p. 279.

[5] J. Shah and R. F. Leheny, in *Semiconductors Probed by Ultrafast Laser Spectroscopy*, edited by R. R. Alfano (Academic, New York, 1984), Vol. 1, p. 45.

[6] A. Mooradian and A. L. McWhorter, in *Proceedings of the 10th International Conference on the Physics of Semiconductors*, edited by S. P. Keller, J. C. Hansel, and F. Stern (U.S. Atomic Energy Commission, Oak Ridge, TN, 1970), p. 380.

[7] S. E. Ralph and G. J. Wolga, Phys. Rev. B **42**, 11 353 (1990).

[8] E. D. Grann, S. J. Sheih, K. T. Tsen, O. F. Sankey, S. E. Günçer, D. K. Ferry, A. Salvador, A. Botcharev, and H. Morkoç, Phys. Rev. B **51**, 1631 (1995).

[9] E. D. Grann, K. T. Tsen, O. F. Sankey, D. K. Ferry, A. Salvador, A. Botcharev, and H. Morkoc, Appl. Phys. Lett. **67**, 1760 (1995).

[10] D. S. Kim and P. Y. Yu, Phys. Rev. B **43**, 4158 (1991).

[11] E. Constant, in *Hot Electron Transport in Semiconductors*, edited by L. Reggiani, Topics in Applied Physics Vol. 58 (Springer-Verlag, Berlin, 1985), p. 227.

[12] D. K. Ferry, H. L. Grubin, and G. J. Iafrate, in *Semiconductors Probed by Ultrafast Laser Spectroscopy*, edited by R. R. Alfano (Academic, New York, 1984), Vol. 1, p. 413.

[13] H. T. Grahn, H. Schneider, and K. von Klitzing, Phys. Rev. B **41**, 2890 (1990).

[14] M. V. Klein, in *Light Scattering in Solids I*, edited by M. Cardona, Topics in Applied Physics Vol. 8 (Springer-Verlag, New York, 1983), p. 151.

[15] G. Abstreiter, M. Cardona, and A. Pinczuk, in *Light Scattering in Solids IV*, edited by M. Cardona and G. Güntherodt, Topics in Applied Physics Vol. 51 (Springer-Verlag, New York, 1983), p. 5.

[16] The assumption that there were negligible SPS contributions beyond 600 cm^{-1} is justified by our ensemble Monte Carlo calculations.

[17] C. Chia, O. F. Sankey, and K. T. Tsen, Mod. Phys. Lett. B **7**, 331 (1993).

[18] See, for example, D. K. Ferry, *Semiconductors* (MacMillan, New York, 1991), Chap. 13.

[19] B. K. Ridley, *Quantum Processes in Semiconductors*, 3rd ed. (Oxford U.P., London, 1993).

[20] T. Yamada, J. R. Zhou, H. Miyata, and D. K. Ferry, IEEE Trans. Electron. Dev. **41**, 1513 (1994).

[21] J. R. Chelikowsky and M. L. Cohen, Phys. Rev. **94**, 1498 (1958).

[22] W. Pötz (private communications).

[23] We note that for a more accurate way of accounting for the non-

parabolicity effects, a more complicated formula resulting from say 16×16 $\mathbf{K}\cdot\mathbf{P}$ perturbation theory should be used. For a comprehensive discussion see, for example, T. Ruf and M. Cardona, Phys. Rev. B **41**, 10 747 (1990) and references therein.

[24] D. Kim, J. M. Jacob, J. F. Zhou, J. J. Song, H. Hou, C. W. Tu, and H. Morkoc, Phys. Rev. B **45**, 13 973 (1992).

[25] J.-Y Bigot, M. T. Portella, R. W. Schoenlein, J. E. Cunningham, and C. V. Shank, Phys. Rev. Lett. **65**, 3429 (1990).

[26] J. Shah, B. Deveaud, T. C. Damen, W. T. Tsang, A. C. Gossard, and P. Lugli, Phys. Rev. Lett. **59**, 2222 (1987).

[27] T. Elsaesser, J. Shah, L. Rota, and P. Lugli, Phys. Rev. Lett. **66**, 1757 (1991).

[28] D. K. Ferry, A. M. Kriman, M.-J. Kann, and R. Joshi, in *Monte Carlo Device Simulations: Full Band and Beyond*, edited by K. Hess (Kluwer Academic, Norwall, MA, 1991), pp. 99–121.

[29] M. J. Kann, A. M. Kriman, and D. K. Ferry, Phys. Rev. B **41**, 12 659 (1990).

[30] A. M. Kriman, M. J. Kann, D. K. Ferry, and R. Joshi, Phys. Rev. Lett. **65**, 1619 (1990).

[31] D. K. Ferry, A. M. Kriman, M.-J. Kann, and R. P. Joshi, Comput. Phys. Commun. **67**, 119 (1991).

[32] P. Lugli, C. Jacoboni, L. Reggiani, and P. Kocevar, Appl. Phys. Lett. **50**, 1251 (1987).